2026 IEEE International Conference on Robotics and Automation (ICRA 2026)
June 1-5, 2026. Vienna, Austria

Stowable Tape Spring Truss Leg for Robotic Mobility

Angelica Peña, Andrew Galassi, and Hannah S. Stuart*

***Abstract*— Obstructed terrains, such as boulders, crevices, and rubble, limit the locomotion of wheeled mobile robots. Transformable wheel-to-leg designs enable better traversal; small wheels provide driving efficiency and deployable legs enable stepping over obstructions. We propose an approach to such leg deployment utilizing a novel tape spring truss structure. It achieves large shape changes – demonstrating transformation ratios from 3.77 to 5.38 between wheel radius and leg length – in a light-weight (8 g) and compact way. Prior tape spring mechanisms have not yet used a string-tensioned truss formation. By tensioning the tape spring via a string mechanism, the wheel's emerging deployable legs are strong enough to traverse obstacles greater than one wheel diameter. Yet, it can also be stowed using just the weight of the rover to coil the tape spring. Adjusting the string pretension allows for optimization of the leg's transverse buckling load, resulting in a strong truss despite low mass and stowed volume. We validate the truss's capability by incorporating it into a two-wheeled mobile rover platform, demonstrating utility in mobility across obstructed terrain.**

I. Introduction

Mobile robots are increasingly deployed in search and rescue, space exploration, and environmental monitoring tasks, where locomotion over unpredictable and obstructed terrain is critical. Traversing obstacles such as boulders, rubble, and crevasses remains an ongoing challenge. Existing mobile systems primarily rely on three modes of locomotion: wheeled, tracked, or legged. While wheeled robots offer speed and efficiency on even ground, they struggle with uneven and granular terrains. Tracked systems are more adaptable to terrains but come with increased energy consumption. Legged robots offer greater mobility for obstructed terrain at the cost of lower speeds and mechanical and control complexity [1].

A. Transforming wheel-legs

Hybrid locomotion systems like those in [2]–[10], and particularly transformable wheel-to-leg designs, have been widely studied to balance these tradeoffs, demonstrating impressive outcomes. These systems leverage the wheels' speed and the legs' adaptability by mechanically switching between configurations through shape change, either actively or passively. A common objective is to maximize leg length change as compared to the original wheel geometry; *transformation ratio* is defined as the ratio between the leg length and the wheel radius. An overview of the state of the art in terms of transformation ratio is shown in Figure 1. The

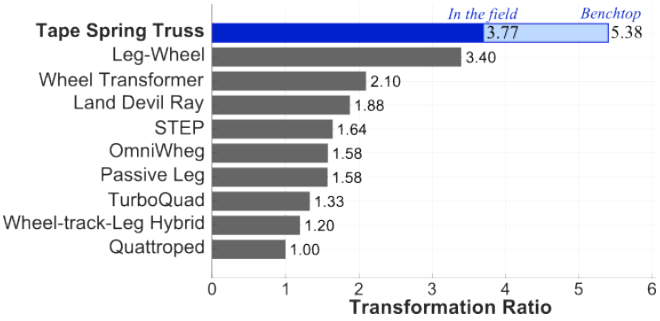

Fig. 1. Transformation ratios of the current work exceed that of prior art, cited from top to bottom: [2] [3] [4] [5] [6] [7] [8] [9] [10].

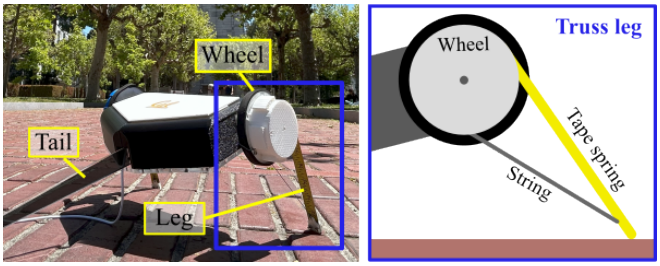

Fig. 2. The tape spring truss legs are deployed on this two-wheeled tail-dragging rover. Here, the legs bear enough transverse load to enable the rover to lift its anterior up off the ground, in order to overcome obstacles in its path. In the deployed state, the truss is made up of a compressed tape spring and a tensioned string.

OmniWheg [6] mechanism achieves a transformed diameter, which determines maximum obstacle traversal height, of less than twice its original diameter. Whereas, the *Leg-Wheel* reaches a transformation ratio of up to 3.4. It translates the wheel axis to the top of the leg, demonstrating the benefit of transforming into a single leg rather than expanding wheel diameter in many directions [2]. To increase transformation ratio further, we propose the first transformable wheel-to-leg mechanism based on a string-tensioned tape spring truss. Our design achieves transformation ratios up to almost 5.4 on benchtop, exceeding prior designs while remaining compact and lightweight. We integrate two of tape spring truss legs, that enable up to 3.77 of transformation ratio, into a two-wheeled tail-dragging rover as seen in Figure 2.

B. Tape spring mechanisms

Tape springs have been previously used in various robotics applications due to their lightweight structure, compact stowage, ability to deploy with stored energy, ability to extend long distances, and anisotropic buckling properties. In robotic manipulators, they have been used as extendable limbs, such as in the climbing robot *EEMMMa* [11], which

All authors are associated with the Department of Mechanical Engineering, University of California, Berkeley.
* Corresponding author: hstuart@berkeley.edu
There is a supplemental video associated with this paper.

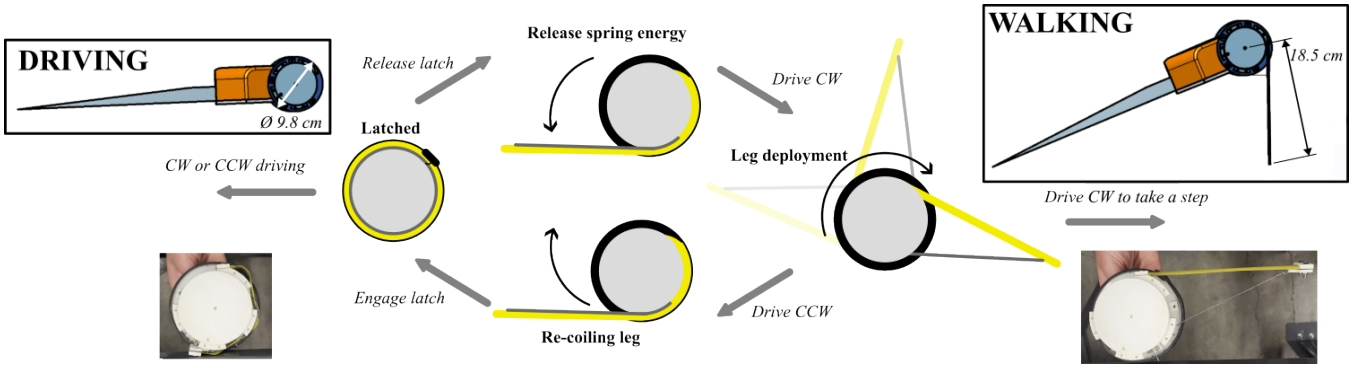

Fig. 3. The overall geometry and dimensions of the stowable tape spring truss rover prototype. The rover is vertically compact, can traverse flat ground efficiently in the wheeled configuration, and can traverse large obstacles disproportionate to its height in the legged configuration.

leverages a tape spring-based limb for vertical motion or *ReachBot* that does so in the horizontal plane [12]. Another manipulator even achieves planar 3 degree-of-freedom reachability [13]. In a gripper-related application, tape springs form flexible surfaces to wrap around objects or as foldable structures to support grasping mechanisms as seen in [14] and [15]; such mechanisms leverage the anisotropic bending properties and the low-energy traveling of bends along the tape spring length once introduced. Beyond robotics, tape springs are widely used in deployable space structures [16], [17], where they serve as supports for antennas, solar arrays, and booms. Notably, they were employed as hinges for the deployable structure for the thermal plasma analyzer in the Japanese Mars orbiter PLANT-B [18]. Across these applications, tape springs are utilized for their unique compliance properties and ability to deform and recover repeatedly.

Multiple configurations for these tape-spring mechanisms exist beyond using just one length. For example, two tape springs deployed together can selectively stiffen a limb to resist any buckling due to transverse loading, even at substantial lengths. Such systems would require an active mechanism to deploy both tape springs. However, in our work, we explore improving tape springs transverse loading capability using an alternative truss formation. Instead of introducing the complexity of two separate tape springs, we reinforce one tape spring in compression with string in tension. As a result, it can deploy by passively releasing its spring energy and be stowed with low forces with the string slack, yet is able to carry the substantial transverse loads necessary for legged locomotion.

C. Overview

The truss mechanism implementation for *whegs* (3.77x wheel-legs transformation) integration into a rover is presented in Section II. An analytical model describing the relationship between extended-leg transverse buckling load capacity as a function of string pretension is presented in Section III. Experiments validate this model (5.38x effective wheel-leg transformation ratio), described in Section IV. The results, in section V, indicate that maximum truss strength occurs when the string length has no slack but little pretension, in between buckling modes, consistent with the predictive model. Presented in Section VI, the rover demonstration validates in the field obstacle traversal using the proposed mechanism for mobility. Discussion of the outcomes and limitations of this work are presented in Section VII, and concluded in Section VIII.

II. Wheg and Rover Implementation

A. Transformable Wheel-to-Leg Design

The transformable wheg design, in both stowed and deployed configurations, is illustrated in Figure 3, as well as the operation to transition between states. The tape spring starts wrapped around the wheel hub and held in place with an actively controlled latch. In this state, the rover drives normally as if with wheels. When the latch is released, the stored spring energy is released, allowing the tape spring to extend. In order for the truss structure to be fully deployed, the wheel must drive in one specific direction until the leg touches the ground and applies tension to the string. The leg is now prepared to take a step. Note that steps can only be taken in the forward direction because driving in the reverse direction then re-coils the leg; the concave side of the tape spring faces inwards toward the wheel so it bends under the weight of the rover. This configuration avoids the need for dedicated actuators for leg deployment and retraction. When re-coiling, the latch is reengaged once fully wrapped to enable normal wheeled driving.

The wheels are 3D printed and incorporate heat-set threaded inserts as mounting points for both the tape spring and string fixture. A braided fishing line rated for 22.7 kg is used, with an approximate calculated stiffness of 10,000 N/m. One end is tied using a Uniknot, while the other is secured with a bolt assembly. The distal end of the tape spring is designed to hold the fishing line knot and create more surface contact with the ground when the leg is deployed. The mass of one entire wheg assembly is 103 g – of which *only 8 g* belongs to the truss mechanism. A stowing latch is driven by a micro-servomotor for demonstration purposes only in the supplemental video, and is not included in this weight estimate.

The tape spring is 17.8 cm long and the stowed wheel has a radius of 4.9 cm; given the truss geometry and integration with the wheel, the effective leg length from wheel axis to foot is 18.5 cm. The resulting transformation ratio is 3.77:1. These dimensions were appropriate and effective for the loads and dimensions of the rover tested, however this transformation ratio is not a fundamental limitation for the truss wheg mechanism, nor did the rover optimize this ratio. Therefore, benchtop experiments and analysis presented in this letter are preformed for a longer tape spring (25.4 cm) as it provides an advantageous 5.38:1 transformation ratio for the same wheel diameter geometry and an effective leg length of 26.4 cm.

B. Tail Dragging Rover Implementation

The design of the rover draws inspiration from prior rovers, like PUFFER [19] and Axel [20], which utilize two-wheeled configuration with a tail or arm to maintain orientation while driving. Our rover features two string-tensioned tape spring whegs and an extended acrylic tail measuring 36 cm in length (total length of the rover in wheel mode is 55 cm). Each wheel is independently actuated by a brushed DC planetary gear motor (ServoCity #638272). The rover body consists of laser-cut acrylic baseplates and a 3D-printed upper shell that houses the electronics. The total mass of the rover is approximately 3.6 kg.

III. Tape Spring Truss Bending Model

The performance of the tape spring trusses during object traversal is dependent on their ability to withstand transverse tip loads without buckling. A key parameter influencing this behavior is the length of the string, which is directly related to the pretension or slack present in the string. Variations in string length lead to corresponding changes in pretension or slack, resulting in a shift in the critical buckling load. Specifically, an excess slack reduces the critical buckling load, while over-tensioning can also lower the load and induce alternative buckling modes. In this section, we develop a predictive model for the transverse buckling load of the tape spring truss as a function of string length variation. Nomenclature is listed in Table I.

The moment of the tape spring is calculated using the Euler-Bernoulli beam theory for a cantilever beam with a point load at the free end, using the following system of equations:

$$M = (F_c - F_s sin(\beta))L + F_s cos(\beta) y \tag{1}$$

$$d = \sqrt{(h+y)^2 + L^2} \tag{2}$$

$$l_0 = d + \delta \tag{3}$$

$$F_s = (d - l_0)k \tag{4}$$

$$y = \frac{(F_c - F_s sin(\beta))L^3}{3EI}. \tag{5}$$

Equation 1 represents the bending moment at the root of the cantilever beam, Equation 2 represents the geometric relationship between the beam deflection and the distance between the beam tip and the string mount, Equation 3 represents the total length of the string before loading, Equation 4 represents the force in the string, and Equation 5 represents the deflection in the beam according to Euler-Bernoulli beam theory.

There are several assumptions relevant to this model, aside from the inherent Euler-Bernoulli approach. We assume the geometry of the deformed tape spring and string are such that the change in the string angle α is small, as shown in Figure 4. Also, we assume the string has a linear relationship between force and deflection, following Hooke's

TABLE I
NOMENCLATURE

Var	Definition	Value/Unit
F_c	Transverse buckling load at the distal end	N
F_s	String tension	N
δ	Slack & displacement of string from init. length	m
β	Angle between horizontal and initial string axis	13.53°
L	Length of tape spring	254 mm
h	Distance between tape spring root and string root	55 mm
y	Deflection of tape spring	m
d	Distance between tape spring tip and string root	235 mm
k	String Stiffness	10778 N/m
E	Modulus of tape spring	190 GPa
I	Moment of inertia of tape spring cross section	$1.3E$-12 m^4
M	Moment of tape spring	N/m
y	Deflection of tape spring	m
l_0	Initial String Length	m
R	Undeformed config. trans. radius of curvature	14.26 mm
t	Thickness of tape spring	0.14 mm
α	Angle of embrace of cross section	75.7°
D	Flexural stiffness of tape spring	0.0471 Nm^2
ν	Poisson's ratio	0.28
n	Notch number	0 to 5

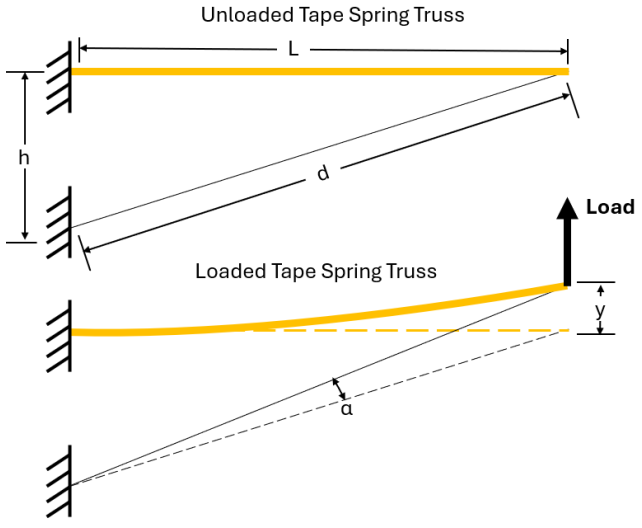

Fig. 4. As the tape spring is loaded, the string (black) is loaded in tension and the tape spring (yellow) is loaded in compression and bending. This truss configuration dramatically increases the transverse load capacity of the structure, compared to a single cantilevered tape spring.

law, however this is only approximately true for a braided string such as that in our ultimate design.

Seffen et. al [21] characterize the maximum bending moments that a tape spring can sustain prior to buckling for both opposite-sense and equal-sense bending. In opposite-sense bending, the longitudinal and transverse curvatures are oriented in the opposing directions, such that the tape cross section experiences a sudden snap-through event at buckling. Whereas, in equal-sense or same-sense bending, both curvatures share the same directional sense, such that the tape gradually bends with increased moment. The critical moment for opposite-sense bending is given by Equation 6, while the maximum moment for equal-sense bending is described in Equation 7. Both of these equations are functions solely of the tape spring's material and geometric properties, as detailed in Equations 8 and 9.

$$M_{+}^{\max} = D\frac{R}{t}\left[\frac{1.152}{10^3} - \frac{2.210}{10^3 l} + \left(-\frac{2.061}{10^9} + \frac{7.096}{10^6 l^4}\left(\frac{R}{t}\right)^2\right)^{\frac{1}{2}}\right]\alpha^{\left[2.840+\frac{18.17}{l^2}+\left(-\frac{2.281}{10^3}+\frac{6.809}{10^2 l}-\frac{0.245}{l^2}\right)\frac{R}{t}\right]} \tag{6}$$

$$\left|M_{-}^{\max}\right| = D\frac{R}{t}\left[\frac{2.600}{10^2} - \frac{2.143}{10^5}\left(\frac{R}{t}\right)\right]\alpha^{\left[2.224+\frac{1.338}{10^3}\frac{R}{t}\right]} \tag{7}$$

$$l = \frac{L}{R\alpha} \tag{8}$$

$$D = Et^3/12(1-\nu^2). \tag{9}$$

Figure 5 shows the resultant bending moments as a function of string slack length. The maximum tip load is determined by the intersection of the moment curve with the critical moment for either same-sense or opposite-sense buckling. A transition to same sense buckling behavior is observed when the slack becomes negative, indicating excessive pretension; in the case of two intersection points, the lower of the points is selected. Under these conditions, the tape spring experiences premature buckling. Critical tip load moments below zero are assumed to be zero, i.e. buckling occurs prior to external loading. As a result, we expect that the 0 mm of slack case to produce the highest critical moment. Higher pretensions result in the tape spring truss exhibiting slight inward bowing prior to external loading. The model captures this effect and highlights the sensitivity of this system to small (on the order of 3mm) changes in string length and the associated string pretension on the tape spring truss strength.

IV. Experimental Setup: Transverse Buckling

An experimental testbed was developed to validate the relationship between string slack and the transverse buckling load of a tape spring, as predicted by our analytical model. As shown in Figure 6, the tape spring is cantilevered from a fixed point. A handheld digital force gauge (Mark-10) is used

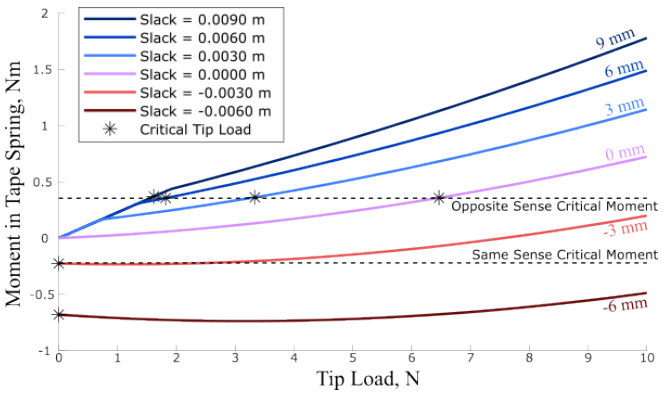

Fig. 5. The analytical model for critical transverse load on the tape spring truss depends on the crossover point between the bending moment in the tape spring for a given transverse tip load, and the critical buckling moment (in opposite-sense or same-sense buckling) of the tape spring. The critical transverse tip load is computed as the intersection between the bending moment curve and the critical moments, for each amount of slack tested in the string.

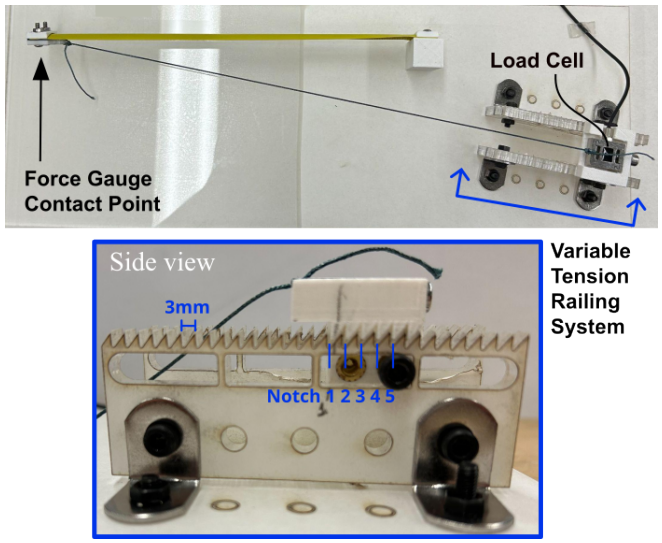

Fig. 6. The model validation experimental setup isolates a single tape spring truss with variable string slack or pretension, and load cell feedback for the string tension. The model validation experimental setup uses a series of discrete notches to repeatably vary the slack or pretension in the truss string.

to apply transverse loading at the end contact point. Only the maximum load is measured as the tape spring undergoes buckling. A string connects from the end of the tape spring to an S-type micro load cell (ATO-LC-S04, 0.1N resolution) for tension measurement. The dimensions of the tape spring and the string attachment angle were fixed to match those described to achieve an effective 5.38:1 wheg transformation ratio in Section II.

To vary string slack, and pretension, the attachment point was adjusted along a series of notched positions on a linear variable tension railing system. Each notch corresponds to a 3 mm increment. At notches 1 and 2, the string has visible slack. Notches below position 1 resulted in excess slack, where the string truss is no longer engaged prior to buckling.

In this condition, the tape spring behaved as an isolated cantilever with a baseline buckling load of 1.4 N. At notch 3, this is the condition closest to the case where slack is 0 mm. Notches 4 and 5 both result in non-zero deflection of the tape spring due to shortened string length. In other words, slack in the string system is varied in discrete increments of 3 mm, denoted by the parameter n:

$$\delta = (3mm) * (3 - n). \tag{10}$$

When n = 3, the string is in its original length constrained by the fixed tape spring's endpoints and the string attachment point. Increasing values of n correspond to negative slack, indicating a pretension. For decreasing n, the slack increases. At n = 0, the string has no effect, and the tape spring behaves as a cantilever beam under transverse loading. Each of the 5 positions were tested for maximum buckling force for 12 trials. A new tape spring, not previously buckled, was used for each notch.

V. Results: Transverse Buckling

A comparison of the beam-buckling model and the experimental data is shown in Figure 7. The overall model trend from notch 0 to notch 3 (as slack is reduced to approximately 0) is similar to the actual buckling loads, with both increasing. This represents the opposite-sense buckling regime for the tape spring. At the nominally zero-slack and zero-pretension notch tested, notch 3, we observed a 557% increase in buckling load relative to the cantilever baseline (notch 0). Thus we confirm that the tape spring truss mechanism using a string improves transverse load bearing capacity. We notice error between the prediction and measurement for notches 1 and 2, such that the model underestimates the measured buckling condition. The measured Notch 3 string pretension was 0.72 N.

Above notch 3, when pretension is deliberately introduced in the string, the model predicts buckling in the same sense direction under 0 N of external load. However, the experiments show nonzero buckling loads. The tape spring begins each trial in the buckled state when initializing the experiments (consistent with the model). When loaded, it experiences unbuckling due to small initially applied loads, then rebuckling at the plotted load, still in the same-sense direction. The model does not capture this secondary buckling behavior accurately. Notch 4 and 5 both measured 0.77N of string pre-tension; this constant force between both notches supports the observation of slight same-sense buckling prior to external loading in this test.

VI. In the Field Demonstration

Fig. 8 presents the rover in its wheeled configuration. Wheeled locomotion is most efficient on flat, non-granular terrain and is operational in this implementation when tested on flat pavement. The rover's obstacle traversal capabilities are demonstrated in Fig. 9 when the legs are deployed, which illustrates successful locomotion over different terrains at a university campus: stairs, a single natural rock, sand,

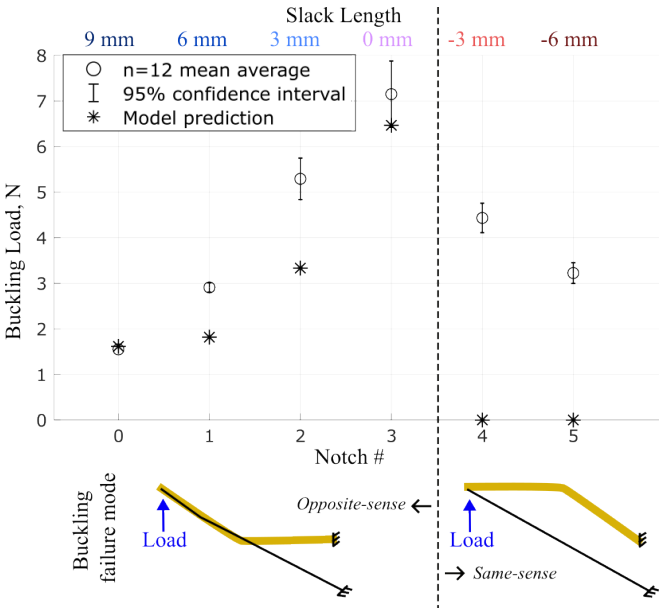

Fig. 7. Experimental measurements of tip buckling load are compared with the model prediction. Corresponding slack length is listed against notch number for clarity.

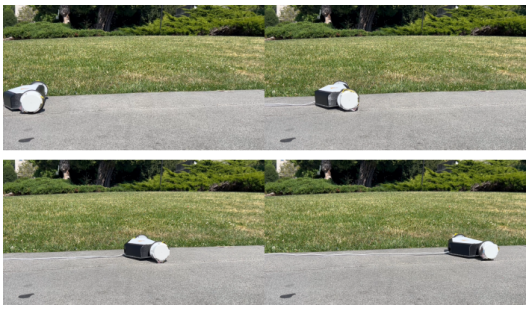

Fig. 8. Stowing the tape spring trusses allows for more energy efficient mobility over flat ground in a wheeled configuration.

and rocky rubble. Wheeled locomotion alone was unable to overcome any of the obstacles in these cases.

Two distinct methods for overcoming obstacles and locomotion emerge for the legged mode across the tested terrains. The tape spring legs are either used to 1) vault over the object with the legs on the ground or 2) pull the rover body upward with the legs on the obstacle. These strategies were discovered through manual joystick control of the two legs, which allowed researchers to experiment with the timing and coordination of motions to achieve mobility. This trial-and-error process was important for success because, if not controlled carefully, the legs may buckle prematurely due to uneven leg loading.

Throughout maneuvers conducted with the tape spring truss legs, the tape springs experience buckling whether during transverse load bearing, or simply when an object contacts with the mid-section of the tape spring or under longitudinal loading. This is seen clearly when the legs make contact with uneven terrains, like the rocks. Provided there

Fig. 9. The stowable tape spring truss rover traversing obstacles such as stairs, rocks, sandy mounds, and rubble, which would otherwise it was not able to traverse in the wheeled setting.

is no permanent deformations or damage caused by these buckling events, the legs are able to recover and continue normal locomotion on the next step. This buckling could be considered a deficit or a benefit of this particular design tape spring truss mechanism, depending on application and use.

VII. Discussion

The most important feature of the model is that it informs how the maximal buckling load for the structure can be achieved, in terms of string length and tension. As anticipated, the best performance occurs when the string does not have slack, but also does not apply substantial pretensions that might prematurely buckle the system when loaded with transverse forces. In real applications, forces may not only be applied in the transverse direction or at the leg tip. However, the field demonstrations shows that the resulting tape spring truss leg can help a rover to overcome obstacles in a less controlled setting.

A. Limitations and Future Work

While we find the model informative, it differs in magnitude from experimental measurements. In part, this may be due to the simplified assumptions regarding string stiffness and negligible orientation change in the string. Thus, it acts as a conservative model, estimating lower failure loads than what was observed. This may also be due to variations of the physical implementation of the prototypes tested, which are not idealized. The model is particularly overly conservative in negative slack cases (notches 4 and 5), indicating that future work should focus on expanding the model to better handle the unbuckling and re-buckling mechanics of this beam loaded.

In the design of the leg truss and the rover, many parameters were selected through trial and error. For example, the tail length was adjusted to enable the legs to lift the body of the rover without buckling. Such relationships between tail length, rover mass, and transverse loads can be modeled in future work to optimize for transformation ratio and rover dimensions. Mobility through more complex terrains may also impact design decision, for example, longer tails could hinder the capability of the rover to maneuver tight spaces with turns and bends, thus making leg selection more complex. The current work utilizes a convenient 2-wheeled rover design that avoids interference between the long deployed legs and additional wheels or the chassis. In a 4-wheeled rover or when the wheels are positioned within the chassis, more constraints on the deployable leg length will limit the transformation ratios achievable with this mechanism.

Future work should also explore control strategies for autonomous legged transitions and driving. Given the potential for the truss to buckle under different loading conditions, this property could either be used on purpose or avoided

using a controller that senses contact forces at the tip and along the leg, e.g., with sensors added for contact feedback. In addition, while we prototyped a preliminary tabletop demonstration of the latching and unlatching mechanism for stowing and releasing the leg, additional engineering integration of a suitable actuator for field operations would allow the automation of this transition, further advancing robotic adaptability in unstructured surroundings. Thus, the feasibility of stowing and deploying this leg mechanisms in different terrains and under varying constraints is yet to be determined.

VIII. Conclusion

In this work, we presented a rover platform featuring transformable wheel-to-leg locomotion, enabled by tape spring trusses. The tail-dragging rover demonstrates the ability to traverse obstructions and challenging terrain, and achieve substantial transformation ratios. A model was developed to relate the maximum transverse buckling load of the tape springs as a function of string slack. We found the model to predict overall trends of force capability, especially identifying the peak capability at the 0-slack condition. Notably, the tape spring truss out performs just the tape spring by more than 5x. The buckling nature of this particular leg design means that the legs can recover even if overloaded, thus providing a useful yet particularly compact and lightweight method of wheg transformation.

ACKNOWLEDGMENT

The work of A. Peña was supported by a National Science Foundation Louis Stokes Alliances for Minority Participation (LSAMP) scholar grant as well as the Cal New Experiences for Research and Diversity in Science (NERDS) program. The work of A. Galassi and H.S. Stuart was supported by a National Aeronautics and Space Administration (NASA) Space Technology Graduate Research Opportunity grant. Any opinions, findings, and conclusions or recommendations expressed in this material are those of the authors and do not necessarily reflect the views of the funding sources. The authors acknowledge the support of the members of the Embodied Dexterity Group.

References

[1] J. M. García and F. G. Duarte, "Mobile rolling robots designed to overcome obstacles: A review," *Forces in Mechanics*, vol. 16, p. 100283, 2024.

[2] H.-Y. Wang, L.-J. Chen, W.-S. Yu, and P.-C. Lin, "A wheel to leg transformation strategy in a leg-wheel transformable robot," in *2023 IEEE/ASME International Conference on Advanced Intelligent Mechatronics (AIM)*, pp. 293–298, IEEE, 2023.

[3] Y.-S. Kim, G.-P. Jung, H. Kim, K.-J. Cho, and C.-N. Chu, "Wheel transformer: A wheel-leg hybrid robot with passive transformable wheels," *IEEE Transactions on Robotics*, vol. 30, no. 6, pp. 1487–1498, 2014.

[4] L. Bai, J. Guan, X. Chen, J. Hou, and W. Duan, "An optional passive/active transformable wheel-legged mobility concept for search and rescue robots," *Robotics and Autonomous Systems*, vol. 107, pp. 145–155, 2018.

[5] Y. Kim, Y. Lee, S. Lee, J. Kim, H. S. Kim, and T. Seo, "Step: A new mobile platform with 2-dof transformable wheels for service robots," *IEEE/ASME Transactions On Mechatronics*, vol. 25, no. 4, pp. 1859–1868, 2020.

[6] R. Cao, J. Gu, C. Yu, and A. Rosendo, "Omniwheg: An omnidirectional wheel-leg transformable robot," in *2022 IEEE/RSJ International Conference on Intelligent Robots and Systems (IROS)*, pp. 5626–5631, IEEE, 2022.

[7] Y. She, C. J. Hurd, and H.-J. Su, "A transformable wheel robot with a passive leg," in *2015 IEEE/RSJ international conference on intelligent robots and systems (IROS)*, pp. 4165–4170, IEEE, 2015.

[8] W.-H. Chen, H.-S. Lin, Y.-M. Lin, and P.-C. Lin, "Turboquad: A novel leg–wheel transformable robot with smooth and fast behavioral transitions," *IEEE Transactions on Robotics*, vol. 33, no. 5, pp. 1025–1040, 2017.

[9] F. Zhou, H. Xu, T. Zou, and X. Zhang, "A wheel-track-leg hybrid locomotion mechanism based on transformable rims," in *2017 IEEE International Conference on Advanced Intelligent Mechatronics (AIM)*, pp. 315–320, IEEE, 2017.

[10] S.-C. Chen, K.-J. Huang, W.-H. Chen, S.-Y. Shen, C.-H. Li, and P.-C. Lin, "Quattroped: a leg–wheel transformable robot," *IEEE/ASME Transactions On Mechatronics*, vol. 19, no. 2, pp. 730–742, 2013.

[11] J. Quan and D. Hong, "Flexible long-reach robotic limbs using tape springs for mobility and manipulation," *Journal of Mechanisms and Robotics*, vol. 15, no. 3, p. 031009, 2023.

[12] T. G. Chen, B. Miller, C. Winston, S. Schneider, A. Bylard, M. Pavone, and M. R. Cutkosky, "Reachbot: A small robot with exceptional reach for rough terrain," in *2022 International Conference on Robotics and Automation (ICRA)*, pp. 4517–4523, 2022.

[13] O. G. Osele, A. M. Okamura, and B. H. Do, "A lightweight, high-extension, planar 3-degree-of-freedom manipulator using pinched bistable tapes," in *2022 International Conference on Robotics and Automation (ICRA)*, pp. 1190–1196, 2022.

[14] G. He, C. Sparks, and N. Gravish, "Grasping and rolling in-plane manipulation using deployable tape spring appendages," *Science Advances*, vol. 11, no. 15, p. eadt5905, 2025.

[15] T. Ding, B. Li, H. Liu, Y. Peng, and Y. Yang, "Planar multi-closed-loop hyper-redundant manipulator using extendable tape springs: Design, modeling, and experiments," *IEEE Robotics and Automation Letters*, vol. 7, no. 3, pp. 6630–6637, 2022.

[16] M. Thaker, S. J. Joshi, H. Arora, and D. B. Shah, "Tape spring for deployable space structures: A review," *Advances in Space Research*, vol. 73, no. 10, pp. 5188–5219, 2024.

[17] A. J. Cook and S. J. Walker, "Experimental research on tape spring supported space inflatable structures," *Acta Astronautica*, vol. 118, pp. 316–328, 2016.

[18] H. Yang, H.-W. Guo, Y. Wang, R.-Q. Liu, and M. Li, "Design and experiment of triangular prism mast with tape-spring hyperelastic hinges," *Chinese Journal of Mechanical Engineering*, vol. 31, no. 1, p. 33, 2018.

[19] I. A. Davydychev, J. T. Karras, and K. C. Carpenter, "Design of a two-wheeled rover with sprawl ability and metal brush traction," *Journal of Mechanisms and Robotics*, vol. 11, no. 3, p. 035002, 2019.

[20] I. A. Nesnas, J. B. Matthews, P. Abad-Manterola, J. W. Burdick, J. A. Edlund, J. C. Morrison, R. D. Peters, M. M. Tanner, R. N. Miyake, B. S. Solish, *et al.*, "Axel and duaxel rovers for the sustainable exploration of extreme terrains," *Journal of Field Robotics*, vol. 29, no. 4, pp. 663–685, 2012.

[21] K. Seffen, S. Pellegrino, and G. Parks, "Deployment of a panel by tape-spring hinges," in *IUTAM-IASS Symposium on Deployable Structures: Theory and Applications: Proceedings of the IUTAM Symposium held in Cambridge, UK, 6–9 September 1998*, pp. 355–364, Springer, 2000.